ACS Sustainable Chemistry & Engineering

pubs.acs.org/journal/ascecg

Research Article

Transformation Kinetics of Phosphorus and Nitrogen in Iron-Rich Sewage Sludges during Hydrothermal Treatment and Recovery of Nutrients from Process Water

Qian Wang, Haesung Jung, Biao Wan, Pan Liu, Peng Yang, and Yuanzhi Tang*

Cite This: *ACS Sustainable Chem. Eng.* 2021, 9, 10630−10641

Read Online

ACCESS | Metrics & More | Article Recommendations | Supporting Information

ABSTRACT: Hydrothermal treatment (HT) is an emerging technique for sustainable sewage sludge management and resource recovery. Many sludges are rich in iron (Fe) due to the common addition of Fe salts in water resource recovery facilities. To develop guidance for reaction conditions targeting nutrient recovery, this study systematically investigated the influence of HT temperature, treatment time, and sludge source on the dynamic speciation evolution of phosphorus (P) and nitrogen (N) during HT of Fe-rich sewage sludge. Complementary chemical extraction and X-ray spectroscopy analyses were conducted to characterize the treatment products. For the sludge mixture (a blend of primary and waste activated sludges), P speciation did not change significantly within 4.5 h at 125 °C HT, while soluble and labile P was converted into insoluble P over time at 175 and 225 °C HT. Strengite ($FePO_4{\cdot}2H_2O$) preferentially formed in the hydrochars with increasing treatment temperature and/or time, whereas 125 °C HT within 1.5 h favored the formation of vivianite ($Fe_3(PO_4)_2{\cdot}8H_2O$). Organic P was completely decomposed into orthophosphate when the HT temperature reached up to 175 °C. Pyrrole-N was enriched in the hydrochars. Similar reaction pathways were observed during HT of anaerobically digested sludge, though some minor differences in Fe-associated P and organic P were observed. Meanwhile, HT of the two sludges released orthophosphate and ammonia into the process waters at 175 and 225 °C, which can be recovered by a sequential process involving struvite ($MgNH_4PO_4{\cdot}6H_2O$) precipitation and air stripping. This study provides new insights into the transformation of P and N during HT of Fe-rich sludges as well as a modular design for maximum P and N recovery from the treatment products.

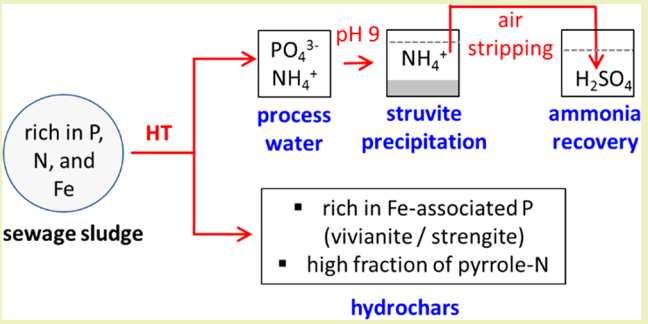

KEYWORDS: *Hydrothermal treatment, Iron-rich sludge, Vivianite, Strengite, Ammonia, Struvite, Air stripping*

INTRODUCTION

The activated sludge process is widely used in water resource recovery facilities (WRRFs) to remove phosphorus (P) and nitrogen (N) from municipal wastewater before discharging it into surface or groundwater.[1,2] The generated byproduct sewage sludge contains high contents of P and N,[3] serving as a good candidate for P and N recycling and reclamation.[4,5] The main forms of P in sewage sludge are orthophosphate (orthoP), organic P, pyrophosphate, and polyphosphate.[6] Almost all of the P in anaerobically digested sludge (ADS) is orthoP,[7,8] whereas 10−30% of the total P exists as organic P in biological sludge.[3] Regarding N, its dominant forms in sewage sludge are inorganic N ions (e.g., ammonia, nitrite, and nitrate) and complex organic N.[9] In recent years, hydrothermal treatment (HT) has emerged as a potentially sustainable technique for sludge management and nutrient reclamation/recycling.[10−12] HT accommodates wet sludge feedstock and produces a slurry that can be separated into solid hydrochar and process water. Hydrochar has been widely evaluated as a soil amendment and fertilizer. For instance, sludge-derived hydrochar with moderately available P (i.e., Fe/Al/Ca-bound P) and residue N (i.e., ammonia) can serve as a slow-release P and N fertilizer.[13,14] Land application of hydrochar rich in aromatic carbon can enhance soil carbon sequestration.[14] Considering that the speciation of P and N determines the efficiency of hydrochars as a soil amendment/fertilizer as well as the nutrient recovery options for the process water, the impacts of the HT temperature, treatment time, and sludge type on the speciation of P and N during HT of sewage sludge warrants systematic investigation.

Prior studies reported that organic P in the sludge was converted into orthoP during HT.[4,15] The final P speciation in

Received: May 23, 2021
Revised: July 10, 2021
Published: July 29, 2021

https://doi.org/10.1021/acssuschemeng.1c03452
ACS Sustainable Chem. Eng. 2021, 9, 10630−10641

Table 1. Sample Labels and Reaction Conditions of Hydrothermal Treatment (HT)[a]

sample label	sample description	HT temp (°C)	HT ramping time (h)	HT holding time (h)	severity factor	pH
SM	sludge mixture					6.02
H125_0.5	HT of SM	125	0.5	0	2.21	5.92
H125_1	HT of SM	125	0.5	0.5	2.51	5.75
H125_1.5	HT of SM	125	0.5	1	2.69	5.71
H125_2.5	HT of SM	125	0.5	2	2.91	5.66
H125_4.5	HT of SM	125	0.5	4	3.17	5.60
H175_0.5	HT of SM	175	0.5	0	3.69	5.66
H175_1	HT of SM	175	0.5	0.5	3.99	5.74
H175_1.5	HT of SM	175	0.5	1	4.16	6.02
H175_2.5	HT of SM	175	0.5	2	4.38	6.10
H175_4.5	HT of SM	175	0.5	4	4.64	6.30
H225_0.5	HT of SM	225	0.5	0	5.16	6.22
H225_1	HT of SM	225	0.5	0.5	5.46	6.50
H225_1.5	HT of SM	225	0.5	1	5.63	6.55
H225_2.5	HT of SM	225	0.5	2	5.86	7.10
H225_4.5	HT of SM	225	0.5	4	6.11	7.56
ADS	anaerobically digested sludge					7.55
AH125_0.5	HT of ADS	125	0.5	0	2.21	8.78
AH125_1	HT of ADS	125	0.5	0.5	2.51	8.84
AH125_1.5	HT of ADS	125	0.5	1	2.69	8.87
AH125_2.5	HT of ADS	125	0.5	2	2.91	8.30
AH125_4.5	HT of ADS	125	0.5	4	3.17	7.95
AH175_0.5	HT of ADS	175	0.5	0	3.69	8.42
AH175_1	HT of ADS	175	0.5	0.5	3.99	8.43
AH175_1.5	HT of ADS	175	0.5	1	4.16	8.19
AH175_2.5	HT of ADS	175	0.5	2	4.38	8.19
AH175_4.5	HT of ADS	175	0.5	4	4.64	8.10
AH225_0.5	HT of ADS	225	0.5	0	5.16	8.54
AH225_1	HT of ADS	225	0.5	0.5	5.46	8.60
AH225_1.5	HT of ADS	225	0.5	1	5.63	8.79
AH225_2.5	HT of ADS	225	0.5	2	5.86	8.80
AH225_4.5	HT of ADS	225	0.5	4	6.11	8.96

[a]Note: All HT experiments had a ramping time of 0.5 h, and the holding time ranged from 0 to 4 h. pH values were measured after HT.

the HT hydrochar is closely related to the type/concentration of metals,[6] HT temperature, and sludge type.[4,15,16] The different physicochemical properties of sludges used in these prior studies[4,6,15,16] resulted in different P speciation evolution pathways during HT. Iron (Fe) is a common and abundant metal ion in sewage sludges, because Fe is present in some wastewaters and/or used as a coagulant for phosphate removal.[7,17] Our recent study showed that HT of Fe-rich sludge at 90 °C (3 h of ramping time and 1 h of holding time) induced the formation of vivianite ($Fe_3(PO_4)_2{\cdot}8H_2O$) in the hydrochars, whereas HT at 155 and 185 °C favored strengite ($FePO_4{\cdot}2H_2O$) formation.[18] Both vivianite and strengite can serve as P fertilizers for enhancing crop yield.[19,20] However, the dynamic evolution of P speciation in Fe-rich sludges during HT remains unclear. Regarding N, peptide-like N in sewage sludge was converted into heterocyclic aromatic N during HT at ≥200 °C,[21,22] and the extent of reaction was highly dependent on the HT temperature rather than treatment time.[22] Prior studies also showed that amino-N in sewage sludge was partially converted to ammonia-N during HT.[23] Moreover, a high HT temperature (up to 320 °C)[11,15,24] and/or long treatment time (up to 16−24 h)[4,6] was commonly employed in previous studies, which requires high energy input for the treatment process. A few previous studies investigated the impacts of low HT temperature (<130 °C) and short treatment time on the evolution of P and N in sewage sludge, but the findings are limited. For instance, previous studies mainly focused on the concentrations of soluble orthoP and ammonia at HT at 120 °C[25] or employed a fixed HT time.[26] For Fe-rich sludges, the dynamic speciation evolution of P and N at a low HT temperature warrants further investigation.

Meanwhile, the HT process water contains high concentrations of orthoP and ammonia, serving as another potential source for the recovery of P and N.[27−29] HT degrades organic P and desorbs orthoP from biomass and minerals surfaces, releasing a portion of the orthoP into the process water.[27,30] NH_3 serves as the major nitrogenous gas during HT, which can be quickly dissolved in the process water.[24] Precipitation of struvite ($MgNH_4PO_4{\cdot}6H_2O$, a slow release fertilizer) is widely used to recover orthoP and ammonia from process water, which is a convenient and effective method for achieving high levels of P recovery.[31] Struvite precipitation requires the presence of orthoP, ammonia, and Mg^{2+} at stoichiometric ratio and an optimal pH range of 8−10,[32] as described by the following equation:

$$Mg^{2+} + NH_4^{+} + PO_4^{3-} + 6H_2O \rightarrow NH_4MgPO_4{\cdot}6H_2O \quad (1)$$

The concentration of ammonia is typically much higher than that of orthoP in the process water.[29] For instance, the molar ratio of ammonia/orthoP in process waters derived from HT of ADS at 160−250 °C (0.5 h) reaches 51−66.[33] Thus, a large

https://doi.org/10.1021/acssuschemeng.1c03452
ACS Sustainable Chem. Eng. 2021, 9, 10630−10641

amount of ammonia still remains in the solution after struvite precipitation, resulting in a low rate of overall ammonia recovery and requiring further targeted recovery of ammonia. Various technologies, including air stripping, forward osmosis, ion exchange, and electrodialysis, have been evaluated to recover ammonia from wastewaters.[9,34−37] Among these technologies, air stripping is highly effective in ammonia recovery from HT process water.[9,34] Especially, prior studies showed high N and P recovery efficiencies for urine via employing the combined processes of air stripping and struvite precipitation.[38,39] Thus, we hypothesize that a sequential struvite precipitation and air stripping process can maximize P and N recovery from HT process water, as the pH range (8−10) for struvite precipitation can be adjusted to facilitate downstream ammonia recovery through air stripping (the pK_a value of NH_3 is 9.25).[9] Given that the presence of Fe inhibits formation of struvite precipitates,[40] it is important to evaluate this sequential process for P/N recovery from HT process water derived from Fe-rich sludges.

To fill the above-mentioned knowledge gaps, the overall goal of this study is twofold: (1) to systematically investigate the speciation of P and N in hydrochar and process water during HT of Fe-rich sewage sludges at relatively low temperature and short duration and (2) to investigate the efficiency of sequential struvite precipitation and air stripping for maximal P and N recovery from the process water derived from Fe-rich sewage sludges. Two types of Fe-rich sewage sludges were studied, a sludge mixture (SM, a blend of primary and waste-activated sludges) and an ADS (note that SM is fed to the on-site anaerobic digesters in most WRRFs). The Fe concentration in SM and ADS is provided in Table S1. HTs were conducted at 125, 175, and 225 °C for up to 4.5 h. Raw sludges (i.e., SM and ADS) and the hydrochars were systematically characterized using chemical extraction, nuclear magnetic resonance (NMR) spectroscopy, synchrotron X-ray diffraction (XRD), P K-edge X-ray absorption near edge structure (XANES) spectroscopy, X-ray photoelectron spectroscopy (XPS), and N isotope analysis. We further evaluated the efficiency of sequential struvite precipitation and air stripping for maximum recovery of orthoP and ammonia from the process waters.

MATERIALS AND METHODS

Sewage Sludge. Two sewage sludges (i.e., SM and ADS) were collected from the F. Wayne Hill Water Resources Center (Buford, GA, U.S.A.). The Center employs an enhanced biological phosphorus removal (EBPR) process, and its detailed treatment procedure is described in our previous studies.[18,41] Collected samples were immediately centrifuged to 10% dry mass [i.e., solid/liquid ratio of 1/9 (w/w)] in the lab. Then, each type of sludge was mixed evenly and stored in the dark at −20 °C without any further pretreatment.

Hydrothermal Treatment. The frozen sludge was thawed at room temperature before HT. SM or ADS (40 g) was loaded into a high-pressure chemical reactor (CIT-HiPR-ST100 model, Col-Int Tech, SC, U.S.A.). The reactor was set up at 125, 175, or 225 °C and heated for 0.5, 1.5, 2.5, or 4.5 h (including ∼0.5 h of ramping time to reach the target temperature). Then, the reactor was allowed to naturally cool down to room temperature. The HT slurries produced at 175 and 225 °C were separated into solids (hydrochar) and supernatants (process water) by centrifugation. Note that HT at 125 °C did not fully convert biomass to hydrochars and resulted in little process water, but the solids were still regarded as hydrochars in this study. A portion of the raw sludges and the produced hydrochars were vacuum freeze-dried until there was no further weight loss and finely ground and stored in a Coy anaerobic chamber (95% N_2/5% H_2; Coy Laboratory Products), to prevent oxidation of the redox-sensitive Fe by air. The dry mass of the raw sludges and hydrochars is provided in Figure S1. Sample labels and HT conditions are detailed in Table 1. The severity factor (SF) is defined by the following equation:

$$\mathrm{SF} = \log(60te^{[(T-100)/14.75]}) \quad (2)$$

where t and T are reaction time (h, including 0.5 h of ramping time) and temperature (°C), respectively.[42] Increasing the HT temperature and time resulted in a high SF (Table 1).

Characterization of Raw Sludges and Hydrochars. *P and N Content Quantification.* Aqua regia digested raw sludges and hydrochars were analyzed for total P content using the molybdate−ascorbic method[43] on an UV−vis spectrophotometer (Carey 60, Agilent). The total N content in the solids was determined using Micro-Dumas combustion analysis on a Carlo Erba NA1500 nitrogen/carbon/sulfur analyzer.

Stable N isotope ($\delta^{15}N$) composition is effectively employed to trace the origin, pathways, and fate of organic N in sludges.[44,45] To investigate the effect of HT on $\delta^{15}N$ changes, $\delta^{15}N$ in the raw sludges and hydrochars was analyzed by the above analyzer paired with a Thermo Scientific Delta V Advantage isotope ratio mass spectrometer using a Thermo Finnigan Conflow III. The $\delta^{15}N$ abundance is expressed as the standard per mil (‰) relative to that of atmospheric N, as defined below:

$$\delta^{15}\mathrm{N} = [(R_{\mathrm{sample}} - R_{\mathrm{standard}}) - 1] \times 1000 \quad (3)$$

where R_{sample} and R_{standard} are the $^{15}N/^{14}N$ (atom%) of the sample and standard, respectively; the standard refers to atmospheric N_2. Samples with positive or negative $\delta^{15}N$ values have heavy or light N isotope signatures, respectively.

Chemical Extraction. Sequential chemical extraction (SCE) of P was conducted on the solid samples according to Hedley's method.[46] Briefly, each solid sample (∼0.15 g) was added to a 50 mL polypropylene centrifuge tube with 20 mL of extraction solution and sequentially extracted for 16 h at room temperature (∼20 °C) on a shaker. Each fraction was defined as (1) readily soluble P (deionized water), (2) exchangeable or loosely sorbed P (0.5 mol/L $NaHCO_3$), (3) Fe/Al-bound P that can be desorbed under alkaline conditions (0.1 mol/L NaOH), (4) insoluble P minerals/salts (1.0 mol/L HCl), and (5) residue, i.e., recalcitrant P (digested by aqua regia).[6,47] The suspension from each extraction step was centrifuged and vacuum-filtered (0.45 μm). Then, a portion of the supernatant was analyzed as inorganic P using the molybdate−ascorbic method. In addition, a portion of the supernatant was further digested by persulfate for determination of total P concentration using the same method. The solid samples were extracted in 2 M KCl,[48] and the ammonia concentration in the extract was determined using the phenate method[48] by UV−vis.

Liquid ^{31}P NMR Spectroscopy. Liquid ^{31}P NMR spectroscopy was used to determine the speciation of extractable P from the raw sludges and their hydrochars. Phosphorus was extracted by reacting the solid samples with a solution containing 0.25 M NaOH and 0.05 M EDTA at a solid/liquid ratio of 1 g per 20 mL for 16 h on a shaker. Then, the extracts were centrifuged, and a portion of supernatant was mixed with D_2O before liquid ^{31}P NMR analysis. The liquid ^{31}P NMR spectra were recorded using a Bruker AMX 400 MHz spectrometer at a resonance frequency of 162 MHz at 297 K.

XRD. The ground solid powders of the raw sludges and hydrochars were subjected to synchrotron XRD, P K-edge XANES, and XPS analyses. For XRD analysis, the solids were packed in polyimide tubing (1 mm i.d., Cole Parmer) and the data was collected at λ = 0.4539 Å with a sample-to-detector distance of 40 cm at Beamline 17-BM-B at the Advanced Photon Source (APS), Argonne National Laboratory, Lemont, IL, U.S.A. The two-dimensional images of the initially collected data were integrated to one-dimensional data using the software GSAS-II.[49] The diffraction pattern of a blank polyimide tubing was subtracted during XRD analyses.

P K-edge XANES. P K-edge XANES spectroscopy was used to determine the relative abundance of different P species. XANES

https://doi.org/10.1021/acssuschemeng.1c03452
ACS Sustainable Chem. Eng. 2021, 9, 10630−10641

spectra were collected on the solids in fluorescence mode using a PIPS detector at Beamline 14-3 at the Stanford Synchrotron Radiation Lightsource (SSRL), Menlo Park, CA, U.S.A. The solids were spread evenly on the adhesive side of P-free Kapton tapes, and the sample chamber was kept under He atmosphere at room temperature during the data collection process. $AlPO_4$ was used for energy calibration by setting the edge position at 2152.8 eV and monitoring possible energy shift during data collection. Data analyses were performed using the software Ifeffit.[50] The standard compounds used for linear combination fitting (LCF) analysis include the following: (1) vivianite, strengite, and phosphate sorbed on ferrihydrite (P-ferrihy), representing Fe-associated P; (2) $AlPO_4$ and phosphate sorbed on γ-alumina (P-alumina), representing Al-associated P; (3) octacalcium phosphate (OctaCa) and hydroxyapatite (HydAp), representing Ca-associated P; (4) phytic acid (PhyAc), representing organic phosphate. Details on the label, source, and spectra of these standard compounds are in Table S2 and Figure S2. Energy was not allowed to float during the LCF analyses. The quality of fitting was assessed by the *R*-factor, and the best fitting results with the lowest *R*-factor values are provided.

XPS. XPS data were collected using a K-Alpha XPS system (Thermo Fisher Scientific) with an Al Kα 1.486 keV source. The C 1s peak (284.6 eV) was used for energy calibration. The spectra were fitted using the software Thermo Avantage and deconvoluted into the following peaks/species: 399.5 ± 0.1 eV (amine-N), 399.9 ± 0.1 eV (amino-N), 400.4 ± 0.1 eV (pyrrolic-N), 401.4 ± 0.1 eV (quaternary-type nitrogen functionalities; quaternary-N),[51] and 402.5 ± 0.1 eV (inorganic N).[9] The N 1s XPS data processing was described in Wang et al.,[52] giving the best fitting accuracies with 3% standard deviation at a 95% confidence level.

Analysis and Recovery of P and N in Process Waters. The concentrations of orthoP, total P, and ammonia in the process waters were determined using the methods described in the Chemical Extraction section. The orthoP concentration in all process water samples was the same as the total P concentration. Considering that HT with longer treatment time (>0.5 h) can decompose more organic P, process water samples at 175 and 225 °C were mixed with D_2O for liquid ^{31}P NMR analysis to confirm that there was no organic P in the process waters. The concentrations of major metals (Ca^{2+}, Mg^{2+}, Al^{3+}, and Fe^{3+}) in the process waters were analyzed by inductively coupled plasma−mass spectrometry (ICP−MS) (Agilent 7500a).

To recover orthoP and ammonia from the process waters, sequential struvite precipitation and air stripping processes were conducted on samples H175_0.5, H225_4.5, AH175_0.5, and AH225_4.5. These four samples were chosen based on the molar ratio of orthoP/ammonia (i.e., end members of each system). Considering that the concentration of orthoP was much lower than that of ammonia, calculated amounts of dissolved Mg^{2+} (as $MgCl_2$) were added into these samples to reach a final concentration equivalent to the total P (Figure 1). The pH was then adjusted to 9 using NaOH to induce struvite precipitation. The precipitated products were collected using 0.45 μm membrane filters, freeze-dried, and analyzed by XRD on a PANalytical Empyrean X-ray diffractometer (Cu Kα radiation, scan step 0.013°, scan rate 1° min^{-1}, 5−85° 2θ). The purity of the precipitated struvite was analyzed using a dissolution method.[53] Briefly, ~50 mg of precipitates was dissolved by a little amount of concentrated HCl, and then the dissolved ammonia and orthoP were determined using the methods described in the Chemical Extraction section. The purity (P) of struvite was calculated by eq 4.

$$P\ (\%) = \frac{n_{\text{ammonia}} M_{\text{struvite}}}{m_{\text{precipitates}}} \times 100\% \tag{4}$$

where n_{ammonia}, M_{struvite}, and $m_{\text{precipitates}}$ are the molar of ammonia, molar mass of struvite, and mass of precipitates, respectively.

Air stripping was employed to further recover the remaining ammonia in the filtrate after struvite precipitation. The pH of the filtrate was adjusted to 10 using NaOH, and the filtrate was continuously bubbled by air. The stripped ammonia was adsorbed by a 1.5 M H_2SO_4 solution to produce ammonia sulfate solution. The removal (Rem) and recovery (Rec) efficiencies of orthoP and ammonia from process waters were calculated by eqs 5 and 6.

$$\text{Rem}\ (\%) = \left(1 - \frac{C_f}{C_0}\right) \times 100\% \tag{5}$$

C_0 and C_f are the initial and final (i.e., after struvite precipitation or air stripping) concentrations of orthoP or ammonia in the solution, respectively.

$$\text{Rec}\ (\%) = \frac{M_r}{M_0} \times 100\% \tag{6}$$

M_0 and M_r are the initial and recovered amounts of orthoP or ammonia in the initial solution and final struvite solids/$(NH_4)_2SO_4$ solution, respectively.

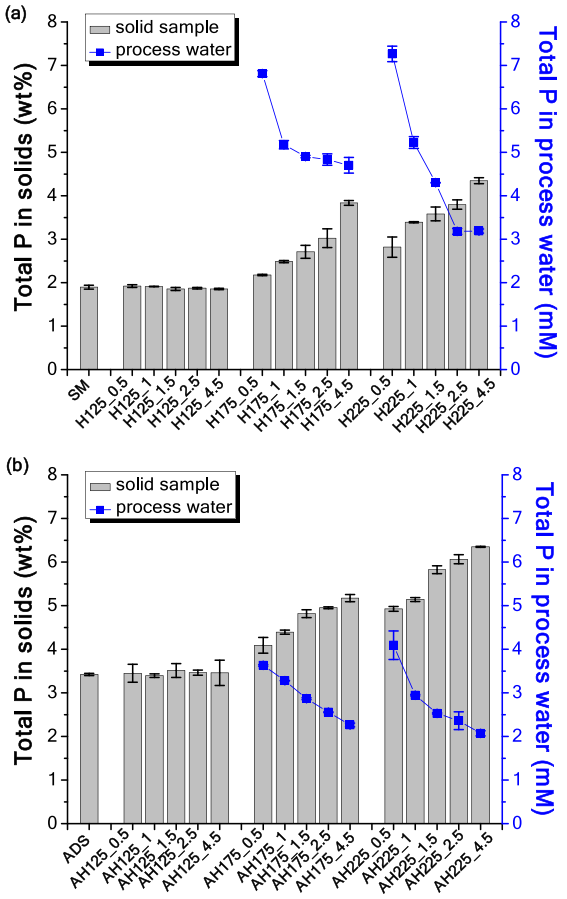

Figure 1. Concentrations of total P in the solid samples (raw sludges and hydrochars) and process waters: (a) sludge mixture (SM); (b) anaerobically digested sludge (ADS).

RESULTS AND DISCUSSION

Speciation Evolution of P in the Hydrochars. *Total P Content.* The total P contents in raw sludge samples SM and ADS are 1.9 wt % (Figure 1a) and 3.3 wt % (Figure 1b), respectively. At 125 °C, the total P content in the hydrochars from both sludges only changed slightly with increasing treatment time as compared to their corresponding raw sludges. Compared with raw sludges, the total P content in the hydrochars from 175 and 225 °C significantly increased. Higher temperature favored P enrichment in the hydrochars. Increasing treatment time at 175 and 225 °C also led to the increase of the total P content in the hydrochars. For SM and

https://doi.org/10.1021/acssuschemeng.1c03452
ACS Sustainable Chem. Eng. 2021, 9, 10630−10641

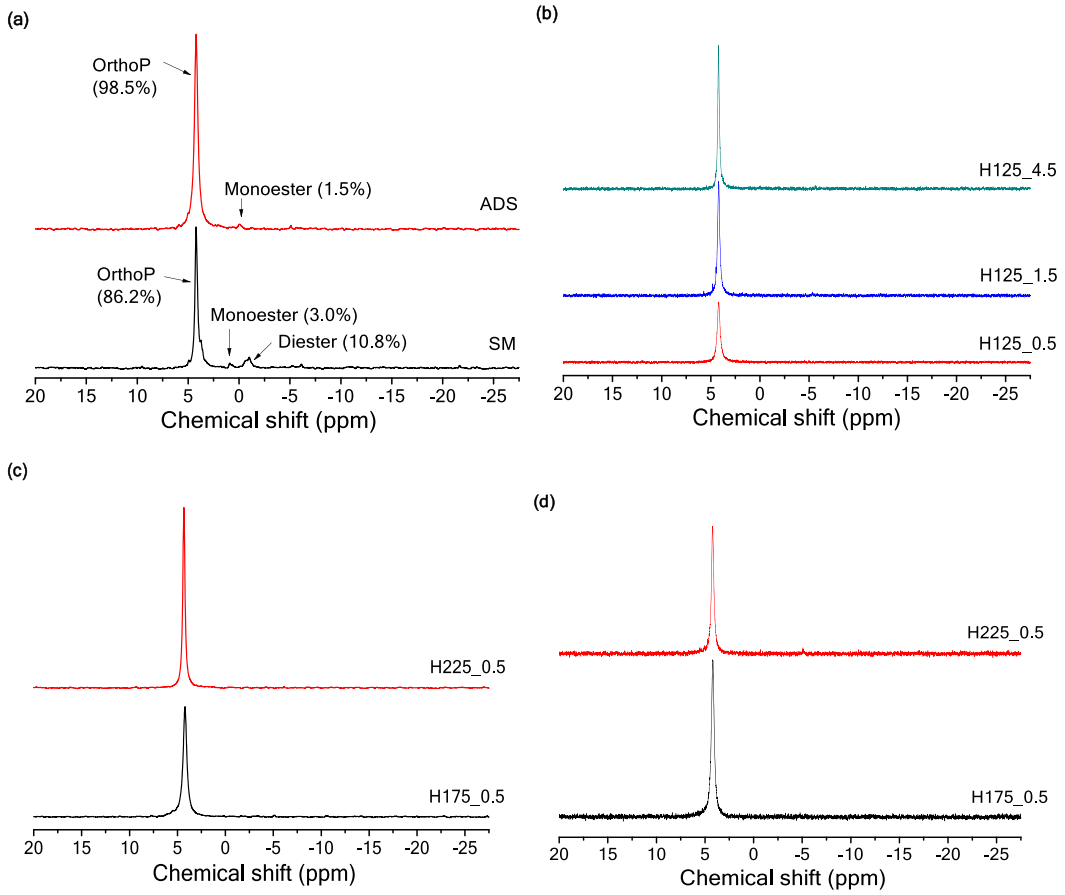

Figure 2. ^{31}P liquid NMR spectra of the extracts from selected samples: (a) sludge mixture (SM) and anaerobically digested sludge (ADS), (b) hydrochars derived from hydrothermal treatment (HT) at 125 °C of SM, (c) hydrochars derived from HT at 175 and 225 °C of SM, and (d) process water for samples H175_0.5 and H225_0.5.

ADS, the highest total P content reached 4.2 wt % for sample H225_4.5 (Figure 1a) and 6.2 wt % for sample AH225_4.5 (Figure 1b), respectively.

Sequential Extraction of P. Figure S3 shows the relative abundance of different P fractions in the extraction solution for the raw sludges and hydrochars. For the SM system (Figure S3a), ∼31% of the P in sample SM was extracted by H_2O and $NaHCO_3$. The NaOH-extractable P fraction accounted for ∼63%, suggesting the high abundance of P associated with Al/Fe minerals. In addition, ∼6% of the P was present in the HCl-extractable and residue fractions. Compared with sample SM, HT at 125 °C did not change the relative abundance of each P species in the hydrochars at different treatment times. Compared to sample SM, HT at 175 and 225 °C decreased the H_2O-, $NaHCO_3$-, and NaOH-extractable fractions in the hydrochars and increased both the HCl-extractable and residue fractions, and such effect was more pronounced with extended treatment time. This suggests that both higher temperature and longer treatment time favored the conversion of soluble and adsorbed P into insoluble P. For instance, the NaOH-extractable, HCl-extractable, and residue fractions of P for sample H225_4.5 were ∼31%, 47%, and 24%, respectively, while the H_2O- and $NaHCO_3$-extractable fractions were negligible. Similar trends (i.e., conversion of soluble and adsorbed P into insoluble P) were observed for P fractions in the hydrochars derived from sample ADS (Figure S3b). Moreover, the H_2O-, $NaHCO_3$-, NaOH-, and HCl-extractable and residue fractions in sample ADS were ∼8%, 14%, 40%, 19%, and 14%, respectively (Figure S3b). The higher fractions of HCl-extractable and residue in sample ADS resulted in a higher insoluble fraction of P in the corresponding hydrochars. For instance, the HCl-extractable and residue fractions for sample AH225_4.5 were ∼50% and 32%, respectively.

Organic P Content. Organic P concentration in the sequential extracts was calculated by the difference between total P and orthoP. The fraction of organic P in sample SM accounted for ∼17% of total P, while it was negligible for sample ADS (Figure S4). For the SM system (Figure S4a), the fraction of organic P decreased to ∼10% for sample H125_0.5 as compared to that in sample SM, but the treatment time ($0.5 < t \leq 4.5$ h) at 125 °C did not induce further degradation of organic P. For all hydrochars derived from at 175 and 225 °C, the fraction of organic P was negligible.

The liquid ^{31}P NMR of the NaOH/EDTA extracts from selected solid samples are also used to determine the organic P content (Figure 2). For the liquid ^{31}P NMR spectrum of the NaOH/EDTA extracts from sample SM (Figure 2a), orthoP was the dominant P species (86.2%) with 10.8% diester-P and 3.0% monoester P. However, there was no appearance of organic P species for the corresponding hydrochars (Figure 2, parts b and c), suggesting that organic P species were fully converted into orthoP at temperatures of >125 °C. For the extracts from sample ADS, only 1.5% monoester P accounted for the organic P species (Figure 2a). The extraction efficiency of NaOH/EDTA (Figure S5) was 92.1% and 69.9% for samples SM and ADS, respectively. For SM, the extraction

https://doi.org/10.1021/acssuschemeng.1c03452
ACS Sustainable Chem. Eng. 2021, 9, 10630−10641

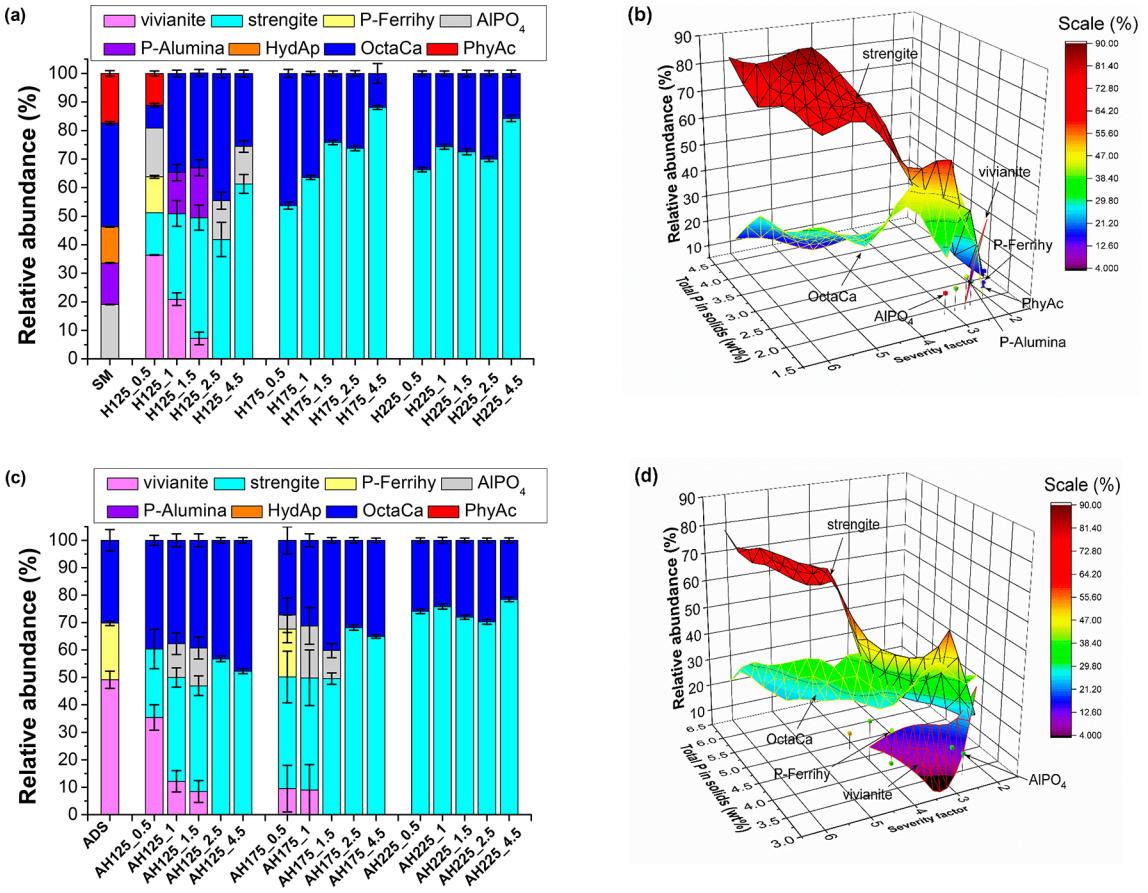

Figure 3. (a and c) Relative abundance of different P species determined from linear combination fitting (LCF) of the P K-edge XANES data of raw sludges and hydrochars: (a) sludge mixture (SM); (c) anaerobically digested sludge (ADS); phosphate sorbed on ferrihydrite (P-ferrihy), phosphate sorbed on γ-alumina (P-alumina), octacalcium phosphate (OctaCa), hydroxyapatite (HydAp), and phytic acid (PhyAc). (b and d) 3D response surface plot of the relative abundance of different P species considering the total P in the solids and the severity factor (SF): (b) SM; (d) ADS.

efficiency for the hydrochars decreased with increasing temperature, due to the high HCl-extractable and residue fractions of P in the hydrochars. For instance, the extraction efficiency was 65.3% for sample H225_0.5, and the HCl-extractable and residue fractions for sample H225_0.5 were 18.1% and 16.1%, respectively.

XRD. To investigate the mineral phase evolution, XRD analysis was conducted on raw sludges and hydrochars (Figure S6). For the SM system (Figure S6a−c), diffraction peaks of quartz and calcite were observed for sample SM. The characteristic peaks of vivianite were present in sample H125_0.5. However, the peaks of vivianite became weaker with increasing treatment time at 125 °C, and these peaks almost completely disappeared for samples H125_2.5 and H125_4.5. Moreover, no vivianite peak appeared for the 175 and 225 °C hydrochars. For the ADS system (Figure S6d−f), we observed the characteristic peaks of vivianite for sample ADS, in addition to the strong diffraction peaks of quartz and calcite. Compared with sample ADS, the intensities of the vivianite diffraction peaks in the 125 °C hydrochars became weaker with increasing treatment time and disappeared at 2.5 h. Similar but faster changes for vivianite diffraction peaks were observed for the 175 °C hydrochars. The vivianite diffraction peaks disappeared after 1 h. Moreover, vivianite was absent in the 225 °C hydrochars.

P XANES. LCF analyses of P K-edge XANES spectra were conducted to quantify P speciation in raw sludges and hydrochars. On the basis of the concentrations of metals (Table S1) and organic P (Figure S4) in raw sludges (samples SM and ADS), a library of P standard compounds including Fe-, Ca-, Al-, and Mg-associated P and organic P were used for LCF analyses. Best fits were obtained using vivianite, strengite, P-ferrihy, $AlPO_4$, P-alumina, HydAp, OctaCa, and PhyAc. For the SM system (Table S3, Figure 3a, and Figure S7a−c), LCF analyses identified $AlPO_4$ (19.1%), P-alumina (14.5%), HydAp (12.7%), OctaCa (36.3%), and PhyAc (17.4%) as the main P species in sample SM. The fraction of PhyAc decreased to 11.1% in sample H125_0.5 as compared to that in sample SM, and no PhyAc was fitted out for the other hydrochar samples. However, P existed predominantly as Fe-associated species in the hydrochar samples. Compared with sample SM, the fractions of vivianite, strengite, and P-ferrihy in sample H125_0.5 increased to 36.4%, 14.8%, and 12.6%, respectively. However, the fraction of vivianite in sample H125_1.5 decreased to 7.2% as compared to that in sample H125_0.5. Furthermore, LCF analysis did not fit out vivianite for H125_2.5, H125_4.5, and the hydrochars derived from 175 and 225 °C, in addition to the adsorbed P species (i.e., P-ferrihy and P-alumina). However, the fraction of strengite in the hydrochars increased with increasing treatment time as compared to that in sample SM. For instance, it was 61.3%,

https://doi.org/10.1021/acssuschemeng.1c03452
ACS Sustainable Chem. Eng. 2021, 9, 10630−10641

88.1%, and 84.2% for samples H125_4.5, H175_4.5, and H225_4.5, respectively. For $AlPO_4$ and Ca-associated P species, their fractions in the hydrochars fluctuated. Figure 3b shows the 3D response surface plot of the relative abundance of different P species considering the total P in the solids and the SF, indicating that enrichment of strengite in the hydrochars was more significant with higher total P in the solids and SF as compared to the hydrochars with lower total P in the solids and SF.

For the ADS system (Table S3, Figure 3c, and Figure S7d−f), vivianite (49.2%), P-ferrihy (20.6%), and OctaCa (30.2%) were identified as the main P species in sample ADS. Note that no organic P species was fitted for sample ADS. These results were consistent with the XRD analysis, showing that organic P species was absent while vivianite was the major P species in ADS.[7,8,54] Compared with sample ADS, the fraction of vivianite decreased in the 125 °C hydrochars with increasing treatment time. No vivianite was observed for samples AH125_2.5 and AH125_4.5. These observations were consistent with the XRD analysis (Figure S6d). In addition, no P-ferrihy species was fitted for the 125 °C hydrochars. However, the fractions of strengite and OctaCa in these hydrochars increased with increasing treatment time as compared to those in sample ADS. For instance, the fractions of strengite and OctaCa in sample AH125_4.5 reached up to 52.3% and 47.7%, respectively. Note that the fraction of $AlPO_4$ in these hydrochars fluctuated. Similar but faster changes on the fractions of vivianite and strengite were observed for 175 °C hydrochars as compared to those in the 125 °C hydrochars. For instance, the fractions of vivianite and strengite in sample AH175_1.5 were 0% and 49.6%, respectively, whereas they were 8.5% and 38.5% for sample AH125_1.5, respectively. For 225 °C hydrochars, strengite and OctaCa were present as major P species. However, HT at 225 °C did not significantly induce the changes on the fractions of strengite and OctaCa with time. The fractions of strengite and OctaCa in these hydrochars remained as ∼74% and ∼26%, respectively. Enrichment of strengite in the hydrochars with high total P in the solids and SF was also observed in the ADS system (Figure 3d), similar as the trend described in the SM system (Figure 3b).

P Speciation Evolution during HT. In order to obtain complementary speciation information of P, we used SCE, NMR, XRD, and XANES methods to characterize the solid samples. The advantages and limitations of each method have been discussed extensively in our previous studies[4,6,18] and are briefly explained below. SCE in this study is used for assessing the mobility and bioavailability of P (i.e., H_2O- and $NaHCO_3$-extractable fractions), although it has the following intrinsic limitations: (1) SCE cannot identify and quantify P associated with specific minerals and (2) P redistribution may occur during extractions. XANES spectroscopy (including LCF analysis) is an *in situ* and nondestructive molecular scale technique which can differentiate Fe/Ca/Al-associated P and organic P in the solid samples. However, it also has intrinsic limitations. For instance, (1) it cannot identify and quantify different organic P species in the solid samples. Thus, we used liquid ^{31}P NMR spectroscopy to identify and quantify various organic P species in the NaOH/EDTA extracts. (2) LCF analysis has a typical error of ∼10% caused by the employment of standard compounds (i.e., a limited standard compound library and similar P XANES spectral features of some standard compounds). Thus, synchrotron-based XRD analysis, sensitive to determine the crystalline P phases, was used to validate the LCF results and reduce the uncertainties.

The speciation evolution of P during HT is highly dependent on the sludge source, the type and concentration of metals with high affinity for P, and the HT temperature and treatment time. The highest-concentration metal in raw sludges is Fe, which is much higher than Ca, Al, and Mg (Table S1), all of which have a strong affinity for P.[40] A series of reactions such as hydrolysis, dehydration, decarboxylation, aromatization, condensation, and polymerization[12] contributed to the decomposition of organic P into inorganic P during the HT of sludge.[6,55,56] For the SM system at 125 °C, vivianite formed in the hydrochars at 0.5−1.5 h, whereas strengite preferentially formed after a treatment time of >1.5 h. High HT temperatures (175 and 225 °C) also favored the formation of strengite in the hydrochars. These observations are consistent with our recent study.[18] Formation of vivianite was due to the reduction of Fe(III) species by furfural derivatives such as 5-hydroxymethylfurfural (5-HMF),[57,58] which are intermediates during the decomposition of cellulose in sewage sludge by HT. However, 5-HMF is unstable at high HT temperatures and can convert into polyaromatic hydrocarbon type compounds by a series of reactions such as polymerization, polycondensation, and aromatization.[59] However, Fe(III) species cannot be easily reduced by the polyaromatic hydrocarbon type compounds. Overall, HT of sewage sludge rich in P and Fe at low temperatures and short treatment times can induce the formation of vivianite in the hydrochars; otherwise, strengite preferentially formed in the hydrochars derived from high temperatures and long treatment times.

For the ADS system, vivianite is a major P species in ADS,[7,54,60−62] which was converted into strengite during HT. Higher temperature and/or longer treatment time favored this conversion, which resulted from the auto-oxidation of vivianite through water decomposition during HT:[63−65]

$$2Fe^{2+} + 2H_2O \rightarrow 2Fe^{3+} + 2OH^- + H_2 \quad (7)$$

Speciation Evolution of N in the Hydrochars. *N Content.* The total N content in the raw sludges and hydrochars is given in Figure 4. The total N content in samples SM and ADS was 5.8 and 5.3 wt %, respectively. Compared with samples SM and ADS, the total N content in the 125 °C hydrochars decreased slightly with increasing treatment time. For instance, the total N content in samples H125_4.5 and AH125_4.5 was 5.5 and 5.0 wt %, respectively. However, the total N content in the 175 and 225 °C hydrochars significantly decreased with increasing treatment time as compared to that in samples SM and ADS. The trends of total N in the 175 and 225 °C hydrochars were opposite to the trends of total P (Figures 2 and 4), consistent with the higher volatility of N than P. The lowest total N content was 3.3 and 2.8 wt % for samples H225_4.5 and AH225_4.5, respectively. The decrease of total N content in the 175 and 225 °C hydrochars was due to release of ammonia into the HT process waters (see below).

The N/C ratios for raw sludges and hydrochars are shown in Figure S8. For the SM system (Figure S8a), the N/C ratio for the 125 °C hydrochars decreased slightly with increasing treatment time as compared to that in sample SM. However, compared to sample SM, a much smaller N/C ratio was observed for the 175 and 225 °C hydrochars. These observations suggested similar volatilization behavior between

https://doi.org/10.1021/acssuschemeng.1c03452
ACS Sustainable Chem. Eng. 2021, 9, 10630−10641

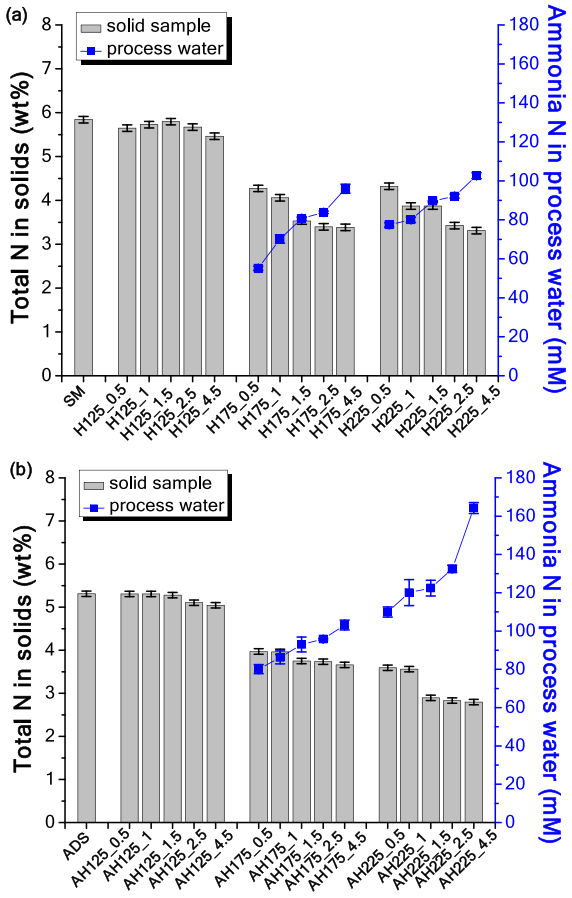

Figure 4. Concentrations of total N and ammonia N in the solid samples and process waters of (a) sludge mixture (SM) and (b) anaerobically digested sludge (ADS).

N and C at lower temperature (i.e., 125 °C), while the volatilization of N was higher than that of C at higher temperatures (i.e., 175 and 225 °C). Moreover, longer treatment time at 175 and 225 °C decreased the N/C ratio for the hydrochars.

The δ^{15}N value for raw sludges and hydrochars was also measured to investigate the effects of HT on the isotopic composition in sewage sludge during HT. N-bearing volatiles such as alkyl, pyrazine, and ammonia have relatively light δ^{15}N values.[45] Figure S9a shows that the δ^{15}N value (3.69‰) in the hydrochars did not significantly change at different HT temperatures (125−225 °C) and treatment times (0−4.5 h) as compared to that for sample SM (3.68‰). It suggests that (1) the contents of the N-bearing volatiles were low in sample SM. In other words, HT within 4.5 h did not induce loss of isotopically light N by volatilization of N-bearing volatiles in sample SM. (2) The produced N-bearing volatiles during HT were mainly released to the liquid and/or gas phases while little N-bearing volatiles were retained in the solids. Similar changes on the N/C ratio and δ^{15}N value were also observed for the ADS system (Figures S8b and S9b), suggesting the above transformation mechanisms of C and N also apply to the ADS system.

Extracted Ammonia. To evaluate the mobility and bioavailability of ammonia in the solid samples, the concentration of extracted ammonia in raw sludges and the hydrochars is given in Figure S10. The concentration of the extracted ammonia in samples SM and ADS was 1.2 and 3.6 mg/g, respectively. For the SM system (Figure S10a), the concentration of the extracted ammonia in all hydrochars was higher than that in sample SM. At 125 °C treatment, this concentration increased with increasing treatment time, reaching 3.4 mg/g for sample H125_4.5. For 175 °C treatment, this concentration decreased from 2.5 mg/g (sample H175_0.5) to 1.5 mg/g (sample H175_4.5). A similar decreasing trend was observed for the 225 °C hydrochars.

For the ADS system (Figure S10b), HT at 125 °C also increased the extracted ammonia concentration in the hydrochars with increasing treatment time as compared to that in sample ADS It reached up to 5.1 mg/g for sample AH125_4.5. However, compared with sample ADS, the concentration of the extracted ammonia in the 175 and 225 °C hydrochars decreased with increasing treatment time. For instance, it was 2.7 and 1.6 mg/g for samples AH175_4.5 and AH225_4.5, respectively.

N XPS Analysis. The N speciation in raw sludges and hydrochars was characterized using N 1s XPS (Figure S11) and peak deconvolution (Figure S12 and Figure 5). For the SM system (Figure 5a), amine-N (25%), amino-N (48%), pyrrole-N (14%), quaternary-N (6%), and inorganic N (7%) were the main N species identified in sample SM. The fraction of amino-N in the 125, 175, and 225 °C hydrochars decreased

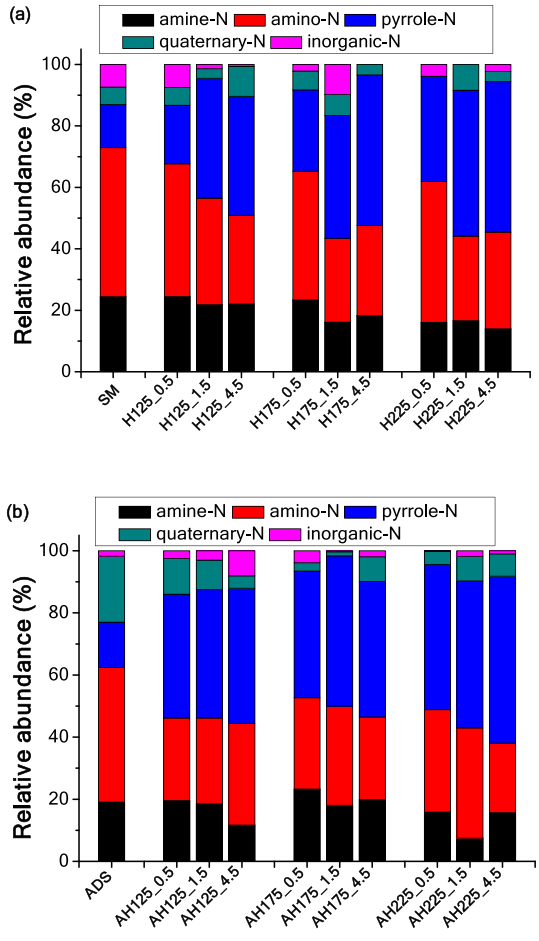

Figure 5. Relative abundance of different N species in the raw sludges and hydrochars determined from deconvolution of the N 1s XPS spectra: (a) sludge mixture (SM); (b) anaerobically digested sludge (ADS).

https://doi.org/10.1021/acssuschemeng.1c03452
ACS Sustainable Chem. Eng. 2021, 9, 10630−10641

as compared to that in sample SM, whereas the fraction of pyrrole-N significantly increased. The fraction of pyrrole-N in the hydrochars from treatment at 1.5 h (125, 175, and 225 °C) was much higher than that from HT at 0.5 h, whereas a treatment time of >1.5 h did not induce more pyrrole-N. Moreover, the fractions of amine-N and quaternary-N in these hydrochars decreased slightly as compared to those in sample SM. For sample H225_4.5, the fractions of amine-N, amino-N, pyrrole-N, quaternary-N, and inorganic N were ∼14%, 31%, 49%, 3%, and 2%, respectively.

For the ADS system (Figure 5b), N existed dominantly as amino-N (43%) in sample ADS, along with around 21% quaternary-N, 19% amine-N, 15% pyrrole-N, and 2% inorganic N. Compared with the SM system, the conversion of amino-N into pyrrole-N in ADS during HT was also observed. However, different treatment times did not have a significant influence on the above conversion. The fraction of quaternary-N in the hydrochars decreased as compared to that in sample ADS. For instance, the fractions of amino-N, quaternary-N, amine-N, pyrrole-N, and inorganic N for sample AH125_4.5 were around 33%, 4%, 12%, 43%, and 8%, respectively.

N Speciation Evolution during HT. The transformation pathways of N in both SM and ADS sludges during HT were similar. Amino-N functional groups in sewage sludge were partially hydrolyzed into ammonia.[23] HT also favored the conversion of amine-N into ammonia.[66] The produced ammonia was released into the process waters, resulting in high ammonia concentration that is suitable for subsequent N recovery (see the Recovery of Nutrients from Process Waters section below). Meanwhile, pyrrole-N functional groups (a type of heterocyclic-N) were enriched in the hydrochars through cyclization and ring condensation reactions during HT.[67,68] This is because pyrrole-N with high thermodynamic stability favored building blocks in the hydrochars.[69] Moreover, pyrrole-N can be formed via reaction of furan with the released ammonia during HT.[69] Some transformation pathways of N proposed by Latham et al.[69] were not observed during our N 1s XPS analysis, probably due to different materials in the two studies (sewage sludges vs N-doped carbon materials). Note that our XPS fitting results mainly reflected the changing trends of N speciation in the hydrochars.

Recovery of Nutrients from Process Waters. For both sludges, HT at 175 and 225 °C led to the release of a portion of the P in the hydrochars into the process waters (Figure 1), and the total P concentration in the process waters decreased with increasing treatment time. Note that the orthoP concentration in all process water samples was the same as the total P concentration, i.e., organic P was absent in the process waters. ^{31}P liquid NMR analyses also confirmed that only orthophosphate existed in the process waters (Figure 2d), consistent with the study by Yu et al.[25] Specifically, for the SM system (Figure 1a), the total P concentration in the process waters decreased from 6.8 mM (sample H175_0.5) to 4.7 mM (sample H175_4.5) at 175 °C treatment, whereas the value decreased from 7.3 mM (sample H225_0.5) to 3.2 mM (sample H225_4.5) for 225 °C treatment. For the ADS system, the total P concentration in the process waters decreased from 3.6 mM (sample AH175_0.5) to 2.3 mM (sample AH175_4.5) and from 4.1 to 2.1 mM for samples AH225_0.5 and AH225_4.5, respectively.

Meanwhile, the concentration of ammonia in the process waters increased with increasing treatment temperature and time (Figure 4). For the SM system (Figure 4a), the concentration of ammonia in the process waters was 55 and 77 mM for samples H175_0.5 and H225_0.5, respectively, whereas it increased to 96 and 103 mM for samples H175_4.5 and H225_4.5, respectively. For the ADS system (Figure 4b), the concentrations of ammonia for samples AH175_0.5 and AH225_0.5 were 77 and 110 mM, respectively. After HT for 4.5 h, it reached up to 92.5 and 160 mM, respectively, for samples AH175_4.5 and AH225_4.5.

After adding Mg^{2+} into the process waters and adjusting the pH value to 9, the precipitated solids were characterized by XRD analyses, which confirmed the formation of struvite (Figure 6). The difference in the relative peak intensity for samples H175_0.5, H225_4.5, AH175_0.5, and AH225_4.5 was observed, due to the different matrixes of the process waters. Compared with samples H175_0.5 and H225_4.5, the intensity of the (002) and (004) peaks for samples AH175_0.5 and AH225_4.5 was much higher. It is likely due to the lower concentrations of Fe, Ca, and Al but higher ammonia concentration in samples AH175_0.5 and AH225_4.5 than those in samples H175_0.5 and H225_4.5 (Table S4 and Figure 4). The presence of metal ions during struvite precipitation was previously shown to strongly decrease struvite crystallinity by inhibiting the growth of the (002) and (004) faces,[40] whereas the presence of a high concentration of ammonia favors the growth of the (002) and (004) faces.[70] The removal and recovery efficiencies of orthoP reached up to ∼99% and ∼98% for all four samples (Table 2), respectively. The purity of the precipitated struvite was 88% and 93% for H175_0.5 and H225_4.5, respectively,

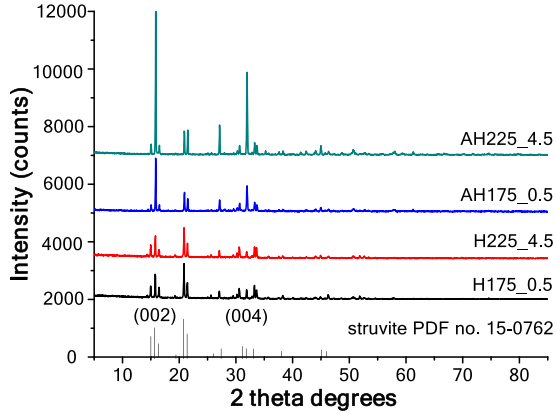

Figure 6. XRD patterns of the precipitated solids from process water samples H175_0.5, H225_4.5, AH175_0.5, and AH225_4.5. The peaks at 16° and 32° correspond to the basal reflections (002) and (004) of struvite, respectively.

Table 2. Removal and Recovery Efficiencies of Orthophosphate and Ammonia from Process Waters, as Well as the Purity of the Precipitated Struvite

	phosphate			ammonia	
sample	removal efficiency (%)	recovery efficiency (%)	*P* (%)	removal efficiency (%)	recovery efficiency (%)
H175_0.5	98.9	98.4	88.1	91.3	83.5
H225_4.5	99.1	98.2	93.3	92.4	83.6
AH175_0.5	99.0	98.3	95.2	92.3	84.1
AH225_4.5	99.4	98.5	95.6	92.2	84.4

https://doi.org/10.1021/acssuschemeng.1c03452
ACS Sustainable Chem. Eng. 2021, 9, 10630−10641

and it reached ~95% for samples AH175_0.5 and AH225_4.5. Subsequently, the removal efficiency of ammonia in the remaining process waters reached up to ~92% for all four samples via the air stripping process, and its recovery efficiency was ~84%, which was lower than the removal efficiency (Table 2). A prior study also observed a portion of ammonia loss during the air stripping process.[39] Note that the recovered ammonia as $(NH_4)_2SO_4$ remained as a liquid phase in this study, similar to previous studies on ammonia recovery by the air stripping process.[38,39]

CONCLUSIONS

This study examined the dynamic transformation of P and N in two types of Fe-rich sewage sludges during HT at different temperatures and treatment times using a range of chemical and spectroscopic methods. The main findings are that (1) HT of both types of Fe-rich sludges favored the formation of strengite in the hydrochars with increasing HT temperature and/or treatment time. HT at 125 °C within 1.5 h also induced the formation of vivianite in the hydrochars. (2) Organic P was completely decomposed at temperatures of ≥175 °C. (3) HT at 125 °C within 4.5 h did not change the bioavailable pools of P (i.e., H_2O- and $NaHCO_3$-extractable fractions) in the hydrochars. HT at high temperatures (175 and 225 °C) and longer treatment times decreased P bioavailability in the hydrochars and orthoP concentration in the process waters. (4) HT induced the enrichment of pyrrole-N functional groups in the hydrochars. (5) HT at 125 °C increased the bioavailability of ammonia (i.e., extractable fraction) in the hydrochars with increasing treatment time, whereas HT at high temperatures (175 and 225 °C) decreased ammonia bioavailability in the hydrochars and released ammonia into the process waters with increasing treatment time. (6) OrthoP and ammonia in the process waters can be recovered by sequential struvite precipitation and air stripping processes. These findings shed light on the evaluation of the potential of hydrochars as biofertilizers during land application. For instance, this study provides information with the mobility and bioavailability of P and ammonia in the hydrochars, which is helpful for understanding the efficiency of hydrochars as a P and N fertilizer. HT at high temperature (i.e., 225 °C) and long treatment time (i.e., 4.5 h) decreased the mobility and bioavailability of P and ammonia in the hydrochars but led to the enrichment of strengite. In addition, vivianite and strengite in the hydrochars can be recovered by magnetic separation.[71] This study also provides strategies on maximum P and N recovery from the process waters using the combination of HT, struvite precipitation, and air stripping processes. HT at high temperature (i.e., 225 °C) and long treatment time (i.e., 4.5 h) favored the recovery of ammonia from the process water. Struvite can serve as an excellent slow-release P fertilizer for enhancing crop yield.[52] The recovered ammonia as $(NH_4)_2SO_4$ solution is also an efficient fertilizer.

ASSOCIATED CONTENT

Supporting Information

The Supporting Information is available free of charge at https://pubs.acs.org/doi/10.1021/acssuschemeng.1c03452.

Dry mass of raw sludges and hydrochars, reference compounds used for P K-edge XANES analysis, results of the major elemental concentrations in the solids and process waters, P fractionation by SCE analysis, XRD analysis, results of P K-edge XANES analysis, stable N isotope ($\delta^{15}N$) analysis, extracted ammonia analysis, and results of N 1s XPS analysis (PDF)

AUTHOR INFORMATION

Corresponding Author

Yuanzhi Tang − *School of Earth and Atmospheric Sciences and School of Civil and Environmental Engineering, Georgia Institute of Technology, Atlanta, Georgia 30332, United States;* orcid.org/0000-0002-7741-8646; Phone: 1-404-894-3814; Email: yuanzhi.tang@eas.gatech.edu

Authors

Qian Wang − *School of Earth and Atmospheric Sciences, Georgia Institute of Technology, Atlanta, Georgia 30332, United States*

Haesung Jung − *School of Earth and Atmospheric Sciences, Georgia Institute of Technology, Atlanta, Georgia 30332, United States; School of Civil, Environmental and Chemical Engineering, Changwon National University, Changwon, Gyeongsangnam-do 51140, Republic of Korea;* orcid.org/0000-0002-8795-248X

Biao Wan − *School of Earth and Atmospheric Sciences, Georgia Institute of Technology, Atlanta, Georgia 30332, United States*

Pan Liu − *School of Earth and Atmospheric Sciences, Georgia Institute of Technology, Atlanta, Georgia 30332, United States*

Peng Yang − *Chemical Sciences and Engineering Division, Argonne National Laboratory, Lemont, Illinois 60439, United States;* orcid.org/0000-0002-5232-7019

Complete contact information is available at: https://pubs.acs.org/10.1021/acssuschemeng.1c03452

Notes

The authors declare no competing financial interest.

ACKNOWLEDGMENTS

This study was supported by the U.S. National Science Foundation under Grant No. 1739884 (Y.T.). Work by P.Y. was supported by the Department of Energy, Office of Science, Office of Basic Energy Sciences, Chemical Sciences, Geosciences, and Biosciences Division. We acknowledge the beamline scientists at Beamline 14-3 at the Stanford Synchrotron Radiation Lightsource (SSRL) and at Beamline 17-BM-B at the Advanced Photon Source (APS) for technical assistance on data collection. This research used resources of the SSRL and APS, U.S. Department of Energy (DOE) Office of Science User Facilities operated under Contract Nos. DE-AC02-76SF00515 and DE-AC02-06CH11357, respectively.

REFERENCES

(1) Law, K. P.; Pagilla, K. R. Reclaimed phosphorus commodity reserve from water resource recovery facilities—A strategic regional concept towards phosphorus recovery. *Resour. Conserv. Recycl.* **2019**, *150*, 104429.

(2) Li, X.; Mei, Q.; Chen, L.; Zhang, H.; Dong, B.; Dai, X.; He, C.; Zhou, J. Enhancement in adsorption potential of microplastics in sewage sludge for metal pollutants after the wastewater treatment process. *Water Res.* **2019**, *157*, 228−237.

(3) Sommers, L. E. Chemical composition of sewage sludges and analysis of their potential use as fertilizers. *J. Environ. Qual.* **1977**, *6* (2), 225−232.

(4) Huang, R.; Tang, Y. Speciation dynamics of phosphorus during (hydro)thermal treatments of sewage sudge. *Environ. Sci. Technol.* **2015**, *49* (24), 14466−14474.
(5) Li, X.; Mei, Q.; Yan, X.; Dong, B.; Dai, X.; Yu, L.; Wang, Y.; Ding, G.; Yu, F.; Zhou, J. Molecular characteristics of the refractory organic matter in the anaerobic and aerobic digestates of sewage sludge. *RSC Adv.* **2018**, *8* (58), 33138−33148.
(6) Huang, R.; Tang, Y. Evolution of phosphorus complexation and mineralogy during (hydro)thermal treatments of activated and anaerobically digested sludge: Insights from sequential extraction and P K-edge XANES. *Water Res.* **2016**, *100*, 439−447.
(7) Wilfert, P.; Dugulan, A. I.; Goubitz, K.; Korving, L.; Witkamp, G. J.; Van Loosdrecht, M. C. M. Vivianite as the main phosphate mineral in digested sewage sludge and its role for phosphate recovery. *Water Res.* **2018**, *144*, 312−321.
(8) Prot, T.; Wijdeveld, W.; Eshun, L. E.; Dugulan, A. I.; Goubitz, K.; Korving, L.; Van Loosdrecht, M. C. M. Full-scale increased iron dosage to stimulate the formation of vivianite and its recovery from digested sewage sludge. *Water Res.* **2020**, *182*, 115911.
(9) He, C.; Wang, K.; Yang, Y.; Amaniampong, P. N.; Wang, J.-Y. Effective nitrogen removal and recovery from dewatered sewage sludge using a novel integrated system of accelerated hydrothermal deamination and air stripping. *Environ. Sci. Technol.* **2015**, *49* (11), 6872−6880.
(10) Raheem, A.; Sikarwar, V. S.; He, J.; Dastyar, W.; Dionysiou, D. D.; Wang, W.; Zhao, M. Opportunities and challenges in sustainable treatment and resource reuse of sewage sludge: A review. *Chem. Eng. J.* **2018**, *337*, 616−641.
(11) Chen, H.; Rao, Y.; Cao, L.; Shi, Y.; Hao, S.; Luo, G.; Zhang, S. Hydrothermal conversion of sewage sludge: Focusing on the characterization of liquid products and their methane yields. *Chem. Eng. J.* **2019**, *357*, 367−375.
(12) Latham, K. G.; Kozyatnyk, I.; Figueira, J.; Carlborg, M.; Rosenbaum, E.; Jansson, S. Self-generation of low ash carbon microspheres from the hydrothermal supernatant of anaerobic digestate: Formation insights and supercapacitor performance. *Chem. Eng. J. Adv.* **2021**, *6*, 100097.
(13) Fei, Y. H.; Zhao, D.; Cao, Y.; Huot, H.; Tang, Y. T.; Zhang, H.; Xiao, T. Phosphorous retention and release by sludge-derived hydrochar for potential use as a soil amendment. *J. Environ. Qual.* **2019**, *48* (2), 502−509.
(14) Zhang, X.; Li, X.; Li, R.; Wu, Y. Hydrothermal carbonization and liquefaction of sludge for harmless and resource purposes: a review. *Energy Fuels* **2020**, *34* (11), 13268−13290.
(15) Shi, Y.; Luo, G.; Rao, Y.; Chen, H.; Zhang, S. Hydrothermal conversion of dewatered sewage sludge: Focusing on the transformation mechanism and recovery of phosphorus. *Chemosphere* **2019**, *228*, 619−628.
(16) Wang, T.; Zhai, Y.; Zhu, Y.; Peng, C.; Wang, T.; Xu, B.; Li, C.; Zeng, G. Feedwater pH affects phosphorus transformation during hydrothermal carbonization of sewage sludge. *Bioresour. Technol.* **2017**, *245*, 182−187.
(17) Wu, H.; Ikeda-Ohno, A.; Wang, Y.; Waite, T. D. Iron and phosphorus speciation in Fe-conditioned membrane bioreactor activated sludge. *Water Res.* **2015**, *76*, 213−226.
(18) Wang, Q.; Zhang, C.; Patel, D.; Jung, H.; Liu, P.; Wan, B.; Pavlostathis, S. G.; Tang, Y. Coevolution of iron, phosphorus, and sulfur speciation during anaerobic digestion with hydrothermal pretreatment of sewage sludge. *Environ. Sci. Technol.* **2020**, *54* (13), 8362−8372.
(19) Fodoué, Y.; Nguetnkam, J.; Tchameni, R.; Basga, S.; Penaye, J. Assessment of the fertilizing effect of vivianite on the growth and yield of the bean 'Phaseolus vulgaris' on oxisoils from Ngaoundere (central north Cameroon). *Int. Res. J. Earth Sci.* **2015**, *3* (4), 18−26.
(20) Ghosh, G. K.; Mohan, K. S.; Sarkar, A. K. Characterization of soil-fertilizer P reaction products and their evaluation as sources of P for gram (Cicer arietinum L.). *Nutr. Cycling Agroecosyst.* **1996**, *46* (1), 71−79.
(21) Liu, T.; Guo, Y.; Peng, N.; Lang, Q.; Xia, Y.; Gai, C.; Liu, Z. Nitrogen transformation among char, tar and gas during pyrolysis of sewage sludge and corresponding hydrochar. *J. Anal. Appl. Pyrolysis* **2017**, *126*, 298−306.
(22) Paneque, M.; De la Rosa, J. M.; Kern, J.; Reza, M. T.; Knicker, H. Hydrothermal carbonization and pyrolysis of sewage sludges: What happen to carbon and nitrogen? *J. Anal. Appl. Pyrolysis* **2017**, *128*, 314−323.
(23) Kruse, A.; Koch, F.; Stelzl, K.; Wüst, D.; Zeller, M. Fate of nitrogen during hydrothermal carbonization. *Energy Fuels* **2016**, *30* (10), 8037−8042.
(24) Zhuang, X.; Huang, Y.; Song, Y.; Zhan, H.; Yin, X.; Wu, C. The transformation pathways of nitrogen in sewage sludge during hydrothermal treatment. *Bioresour. Technol.* **2017**, *245*, 463−470.
(25) Yu, Y.; Lei, Z.; Yuan, T.; Jiang, Y.; Chen, N.; Feng, C.; Shimizu, K.; Zhang, Z. Simultaneous phosphorus and nitrogen recovery from anaerobically digested sludge using a hybrid system coupling hydrothermal pretreatment with MAP precipitation. *Bioresour. Technol.* **2017**, *243*, 634−640.
(26) Fang, C.; Huang, R.; Dykstra, C.; Jiang, R.; Pavlostathis, S. G.; Tang, Y. Energy and nutrient recovery from sewage sludge and manure via anaerobic digestion with hydrothermal pretreatment. *Environ. Sci. Technol.* **2020**, *54* (2), 1147−1156.
(27) Marin-Batista, J. D.; Mohedano, A. F.; Rodríguez, J. J.; de la Rubia, M. A. Energy and phosphorous recovery through hydrothermal carbonization of digested sewage sludge. *Waste Manage.* **2020**, *105*, 566−574.
(28) Idowu, I.; Li, L.; Flora, J. R. V.; Pellechia, P. J.; Darko, S. A.; Ro, K. S.; Berge, N. D. Hydrothermal carbonization of food waste for nutrient recovery and reuse. *Waste Manage.* **2017**, *69*, 480−491.
(29) Wang, M.; Zhang, B.; Cai, C.; Xin, Y.; Liu, H. Acidic hydrothermal treatment: Characteristics of organic, nitrogen and phosphorus releasing and process optimization on lincomycin removal from lincomycin mycelial residues. *Chem. Eng. J.* **2018**, *336*, 436−444.
(30) Li, S.; Zeng, W.; Jia, Z.; Wu, G.; Xu, H.; Peng, Y. Phosphorus species transformation and recovery without apatite in FeCl3-assisted sewage sludge hydrothermal treatment. *Chem. Eng. J.* **2020**, *399*, 125735.
(31) Becker, G. C.; Wüst, D.; Köhler, H.; Lautenbach, A.; Kruse, A. Novel approach of phosphate-reclamation as struvite from sewage sludge by utilising hydrothermal carbonization. *J. Environ. Manage.* **2019**, *238*, 119−125.
(32) Barbosa, S. G.; Peixoto, L.; Meulman, B.; Alves, M. M.; Pereira, M. A. A design of experiments to assess phosphorous removal and crystal properties in struvite precipitation of source separated urine using different Mg sources. *Chem. Eng. J.* **2016**, *298*, 146−153.
(33) Aragón-Briceño, C.; Ross, A. B.; Camargo-Valero, M. A. Evaluation and comparison of product yields and bio-methane potential in sewage digestate following hydrothermal treatment. *Appl. Energy* **2017**, *208*, 1357−1369.
(34) Huang, W.; Yuan, T.; Zhao, Z.; Yang, X.; Huang, W.; Zhang, Z.; Lei, Z. Coupling hydrothermal treatment with stripping technology for fast ammonia release and effective nitrogen recovery from chicken manure. *ACS Sustainable Chem. Eng.* **2016**, *4* (7), 3704−3711.
(35) Iddya, A.; Hou, D.; Khor, C. M.; Ren, Z.; Tester, J.; Posmanik, R.; Gross, A.; Jassby, D. Efficient ammonia recovery from wastewater using electrically conducting gas stripping membranes. *Environ. Sci.: Nano* **2020**, *7* (6), 1759−1771.
(36) Ray, H.; Perreault, F.; Boyer, T. H. Ammonia recovery from hydrolyzed human urine by forward osmosis with acidified draw solution. *Environ. Sci. Technol.* **2020**, *54* (18), 11556−11565.
(37) Huang, W.; Huang, W.; Yuan, T.; Zhao, Z.; Cai, W.; Zhang, Z.; Lei, Z.; Feng, C. Volatile fatty acids (VFAs) production from swine manure through short-term dry anaerobic digestion and its separation from nitrogen and phosphorus resources in the digestate. *Water Res.* **2016**, *90*, 344−353.

https://doi.org/10.1021/acssuschemeng.1c03452
ACS Sustainable Chem. Eng. 2021, 9, 10630−10641

(38) Xu, K.; Zhang, C.; Li, J.; Cheng, X.; Wang, C. Removal and recovery of N, P and K from urine via ammonia stripping and precipitations of struvite and struvite-K. *Water Sci. Technol.* **2017**, *75* (1), 155−164.
(39) Wei, S. P.; van Rossum, F.; van de Pol, G. J.; Winkler, M.-K. H. Recovery of phosphorus and nitrogen from human urine by struvite precipitation, air stripping and acid scrubbing: A pilot study. *Chemosphere* **2018**, *212*, 1030−1037.
(40) Yan, H.; Shih, K. Effects of calcium and ferric ions on struvite precipitation: A new assessment based on quantitative X-ray diffraction analysis. *Water Res.* **2016**, *95*, 310−318.
(41) Wang, Q.; Zhang, C.; Liu, P.; Jung, H.; Wan, B.; Patel, D.; Pavlostathis, S. G.; Tang, Y. Effect of inter-stage hydrothermal treatment on anaerobic digestion of sewage sludge: Speciation evolution of phosphorus, iron, and sulfur. *ACS Sustainable Chem. Eng.* **2020**, *8* (44), 16515−16525.
(42) Heidari, M.; Norouzi, O.; Salaudeen, S.; Acharya, B.; Dutta, A. Prediction of hydrothermal carbonization with respect to the biomass components and severity factor. *Energy Fuels* **2019**, *33* (10), 9916−9924.
(43) Kahiluoto, H.; Kuisma, M.; Ketoja, E.; Salo, T.; Heikkinen, J. Phosphorus in manure and sewage sludge more recyclable than in soluble inorganic fertilizer. *Environ. Sci. Technol.* **2015**, *49* (4), 2115−2122.
(44) Savage, C. Tracing the influence of sewage nitrogen in a coastal ecosystem using stable nitrogen isotopes. *Ambio* **2005**, *34* (2), 145−150.
(45) Toufiq Reza, M.; Poulson, S. R.; Román, S.; Coronella, C. J. Behavior of stable carbon and stable nitrogen isotopes during hydrothermal carbonization of biomass. *J. Anal. Appl. Pyrolysis* **2018**, *131*, 85−92.
(46) Hedley, M. J.; Stewart, J. W. B.; Chauhan, B. S. Changes in inorganic and organic soil phosphorus fractions induced by cultivation practices and by laboratory incubations. *Soil Sci. Soc. Am. J.* **1982**, *46* (5), 970−976.
(47) Levy, E. T.; Aschlesinger, W. H. A comparison of fractionation methods for forms of phosphorus in soils. *Biogeochemistry* **1999**, *47* (1), 25−38.
(48) Dorich, R. A.; Nelson, D. W. Direct colorimetric measurement of ammonium in potassium chloride extracts of soils. *Soil Sci. Soc. Am. J.* **1983**, *47* (4), 833−836.
(49) Toby, B. H.; Von Dreele, R. B. GSAS-II: the genesis of a modern open-source all purpose crystallography software package. *J. Appl. Crystallogr.* **2013**, *46* (2), 544−549.
(50) Ravel, B.; Newville, M. ATHENA, ARTEMIS, HEPHAESTUS: data analysis for X-ray absorption spectroscopy using IFEFFIT. *J. Synchrotron Radiat.* **2005**, *12* (4), 537−541.
(51) Kelemen, S. R.; Freund, H.; Gorbaty, M. L.; Kwiatek, P. J. Thermal chemistry of nitrogen in kerogen and low-rank coal. *Energy Fuels* **1999**, *13* (2), 529−538.
(52) Wang, Q.; Liu, X.; Jung, H.; Zhao, S.; Pavlostathis, S. G.; Tang, Y. Effect of prestage hydrothermal treatment on the formation of struvite vs vivianite during semicontinuous anaerobic digestion of sewage sludge. *ACS Sustainable Chem. Eng.* **2021**, *9* (27), 9093−9105.
(53) Hao, X.-D.; Wang, C.-C.; Lan, L.; Van Loosdrecht, M. Struvite formation, analytical methods and effects of pH and Ca^{2+}. *Water Sci. Technol.* **2008**, *58* (8), 1687−1692.
(54) Wilfert, P.; Mandalidis, A.; Dugulan, A. I.; Goubitz, K.; Korving, L.; Temmink, H.; Witkamp, G. J.; Van Loosdrecht, M. C. M. Vivianite as an important iron phosphate precipitate in sewage treatment plants. *Water Res.* **2016**, *104*, 449−460.
(55) Zheng, X.; Jiang, Z.; Ying, Z.; Ye, Y.; Chen, W.; Wang, B.; Dou, B. Migration and transformation of phosphorus during hydrothermal carbonization of sewage sludge: Focusing on the role of pH and calcium additive and the transformation mechanism. *ACS Sustainable Chem. Eng.* **2020**, *8* (21), 7806−7814.
(56) Funke, A.; Ziegler, F. Hydrothermal carbonization of biomass: a summary and discussion of chemical mechanisms for process engineering. *Biofuels, Bioprod. Biorefin.* **2010**, *4* (2), 160−177.
(57) Gu, L.; Li, B.; Wen, H.; Zhang, X.; Wang, L.; Ye, J. Co-hydrothermal treatment of fallen leaves with iron sludge to prepare magnetic iron product and solid fuel. *Bioresour. Technol.* **2018**, *257*, 229−237.
(58) Jiang, Y.; Yang, L.; Bohn, C. M.; Li, G.; Han, D.; Mosier, N. S.; Miller, J. T.; Kenttämaa, H. I.; Abu-Omar, M. M. Speciation and kinetic study of iron promoted sugar conversion to 5-hydroxymethylfurfural (HMF) and levulinic acid (LA). *Org. Chem. Front.* **2015**, *2* (10), 1388−1396.
(59) Shi, N.; Liu, Q.; He, X.; Wang, G.; Chen, N.; Peng, J.; Ma, L. Molecular structure and formation mechanism of hydrochar from hydrothermal carbonization of carbohydrates. *Energy Fuels* **2019**, *33* (10), 9904−9915.
(60) Wilfert, P.; Kumar, P. S.; Korving, L.; Witkamp, G.-J.; van Loosdrecht, M. C. M. The relevance of phosphorus and iron chemistry to the recovery of phosphorus from wastewater: A review. *Environ. Sci. Technol.* **2015**, *49* (16), 9400−9414.
(61) Wu, Y.; Luo, J.; Zhang, Q.; Aleem, M.; Fang, F.; Xue, Z.; Cao, J. Potentials and challenges of phosphorus recovery as vivianite from wastewater: A review. *Chemosphere* **2019**, *226*, 246−258.
(62) Roussel, J.; Carliell-Marquet, C. Significance of vivianite precipitation on the mobility of iron in anaerobically digested sludge. *Front. Environ. Sci.* **2016**, *4* (60), 1−12.
(63) Hanzel, D.; Meisel, W.; Hanzel, D.; Gütlich, P. Mössbauer effect study of the oxidation of vivianite. *Solid State Commun.* **1990**, *76* (3), 307−310.
(64) McCammon, C. A.; Burns, R. G. The oxidation mechanism of vivianite as studies by Möessbauer spectroscopy. *Am. Mineral.* **1980**, *65* (3−4), 361−366.
(65) Pratt, A. R. Vivianite auto-oxidation. *Phys. Chem. Miner.* **1997**, *25* (1), 24−27.
(66) Tian, K.; Liu, W.-J.; Qian, T.-T.; Jiang, H.; Yu, H.-Q. Investigation on the evolution of N-containing organic compounds during pyrolysis of sewage sludge. *Environ. Sci. Technol.* **2014**, *48* (18), 10888−10896.
(67) Tian, Y.; Zhang, J.; Zuo, W.; Chen, L.; Cui, Y.; Tan, T. Nitrogen conversion in relation to NH3 and HCN during microwave pyrolysis of sewage sludge. *Environ. Sci. Technol.* **2013**, *47* (7), 3498−3505.
(68) Zhang, B.; Xiong, S.; Xiao, B.; Yu, D.; Jia, X. Mechanism of wet sewage sludge pyrolysis in a tubular furnace. *Int. J. Hydrogen Energy* **2011**, *36* (1), 355−363.
(69) Latham, K. G.; Simone, M. I.; Dose, W. M.; Allen, J. A.; Donne, S. W. Synchrotron based NEXAFS study on nitrogen doped hydrothermal carbon: Insights into surface functionalities and formation mechanisms. *Carbon* **2017**, *114*, 566−578.
(70) Shaddel, S.; Ucar, S.; Andreassen, J.-P.; Østerhus, S. W. Engineering of struvite crystals by regulating supersaturation - Correlation with phosphorus recovery, crystal morphology and process efficiency. *J. Environ. Chem. Eng.* **2019**, *7* (1), 102918.
(71) Prot, T.; Nguyen, V. H.; Wilfert, P.; Dugulan, A. I.; Goubitz, K.; De Ridder, D. J.; Korving, L.; Rem, P.; Bouderbala, A.; Witkamp, G. J.; van Loosdrecht, M. C. M. Magnetic separation and characterization of vivianite from digested sewage sludge. *Sep. Purif. Technol.* **2019**, *224*, 564−579.

https://doi.org/10.1021/acssuschemeng.1c03452
ACS Sustainable Chem. Eng. 2021, 9, 10630−10641